

## Dense Alkyne Arrays of a Zr(IV) Metal–Organic Framework Absorb $\text{Co}_2(\text{CO})_8$ for Functionalization

Yingxue Diao, Jieying Hu, Shengxian Cheng, Feixiang Ma, Mu-Qing Li, Xiangzi Hu, Yang Yang Li, Jun He,\* and Zhengtao Xu\*



Cite This: <https://dx.doi.org/10.1021/acs.inorgchem.0c00328>



Read Online

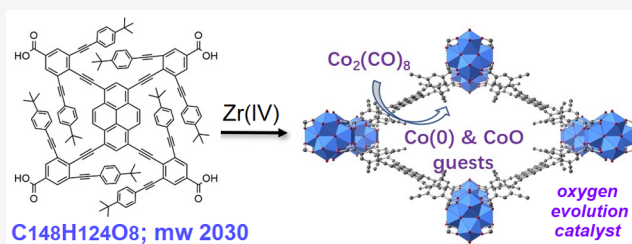
ACCESS |

Metrics & More

Article Recommendations

Supporting Information

**ABSTRACT:** Finely dispersed Co(0) and CoO species were efficiently loaded into a stable metal–organic framework to impart catalytic activities to the porous solid. The metalation of the MOF host is facilitated by the dense arrays of accessible alkyne units that boost the alkyne- $\text{Co}_2(\text{CO})_8$  interaction. The tetrakis(4-carboxylphenylethynyl)pyrene linker, with eight symmetrically backfolded alkyne side arms, features strong fluorescence and a dendritic Sierpinski shape. The resultant Zr(IV)-MOF features NU-901 topology (scu net, with rhombus channels) and breathing properties (e.g., the contracted (porous) phase reverts to the as-made phase upon contact with DMF (dimethylformamide)). The inserted  $\text{Co}_2(\text{CO})_8$  guests quickly react with air to form atomically dispersed CoO species (nondiffracting), and subsequent thermal treatment at 600 °C of the CoO-loaded solid generates an electrocatalyst for the oxygen evolution reaction (OER).



The metalation of metal–organic framework (MOF) materials closely impacts the topical areas of heavy metal removal,<sup>1–6</sup> heterogeneous catalysis,<sup>7–17</sup> sensors,<sup>18–20</sup> and fundamental studies of crystal structures<sup>21–26</sup> because of the versatile functions that can arise from the metal guests. To facilitate metal uptake, MOF hosts are often equipped with secondary donor groups, in addition to the primary groups for network construction. To prevent the secondary groups from competing against the primary linking units (and disrupting the formation of the host net), the difference in chemical hardness is important. An early work<sup>9</sup> utilized a pyridinyl (soft) linker equipped with phenol (hard) groups: the pyridinyls and Cd(II) ions first form the open net; the hydroxyl units then bind Ti(IV) guests for catalysis. More distinct hard-and-soft design has also been extensively implemented in the form of the carboxyl–sulfur combination.<sup>4,22,27–29</sup>

In this context, the alkyne function presents a curious case. On the one hand, alkyne units, as chemically soft groups, are known to form  $\pi$ -complexes (e.g., via  $\eta^2$ -alkyne bonds) with soft metal centers such as Ag(I) and Au(I);<sup>30–34</sup> alkyne groups are also reacted with  $\text{Co}_2(\text{CO})_8$ ,  $\text{Fe}_3(\text{CO})_{12}$ , and other metal carbonyls to form complexes in solution chemistry investigations.<sup>35,36</sup> On the other hand, alkyne groups have been largely left out as secondary donors for metal uptake in the design of MOF materials. Such scarcity is surprising, as alkyne groups generally withstand the solvothermal conditions of MOF synthesis: cases are known where the alkyne units are built into side chains branching off the MOF backbone and are therefore poised to act as secondary donors.<sup>37</sup>

To exploit alkyne–metal interactions for functionalizing porous materials, here we report a designer linker featuring a

dense and symmetrical array of alkyne functions ( $\text{H}_4\text{L}1$ ; Figure 1A). The geometric design of  $\text{H}_4\text{L}1$  follows our long-standing interest<sup>38–43</sup> in the self-similar feature of Sierpinski molecules, with their distinct, symmetrically backfolded side arms<sup>44–50</sup> contrasting the starburst shape of traditional dendrimers. The 1,2,3-positions of the contiguous alkyne units in this Sierpinski molecule facilitate metal uptake, not only because of their dense, chelation-prone array but also because of the spatial accessibility of the flanking alkyne units. For these are freer than the (middle) backbone alkyne unit, i.e., freer to move about, and also to accommodate the geometric changes entailed in bonding to metal centers. To solubilize the large, pyrene-based conjugate backbone, *tert*-butyl groups are appended to the side arms. The  $\text{H}_4\text{L}1$  molecule thus designed and synthesized reacts with Zr(IV) ions to form a porous 3D net that effectively takes up cobalt guests, which, even after carbonizing at 600 °C, remain finely dispersed and afford distinct catalytic activity for oxygen evolution reactions.

The orange, polycrystalline powder of  $\text{ZrL}1$  was solvothermally prepared from  $\text{H}_4\text{L}1$ ,  $\text{ZrOCl}_2 \cdot 8\text{H}_2\text{O}$ , *N,N*-diethylformamide (DEF, the solvent), and benzoic acid (the modulator). Powder X-ray diffraction (PXRD) reveals an orthorhombic symmetry ( $a = 42.10$ ,  $b = 24.02$ , and  $c = 19.19$  Å; pattern b,

Received: February 1, 2020

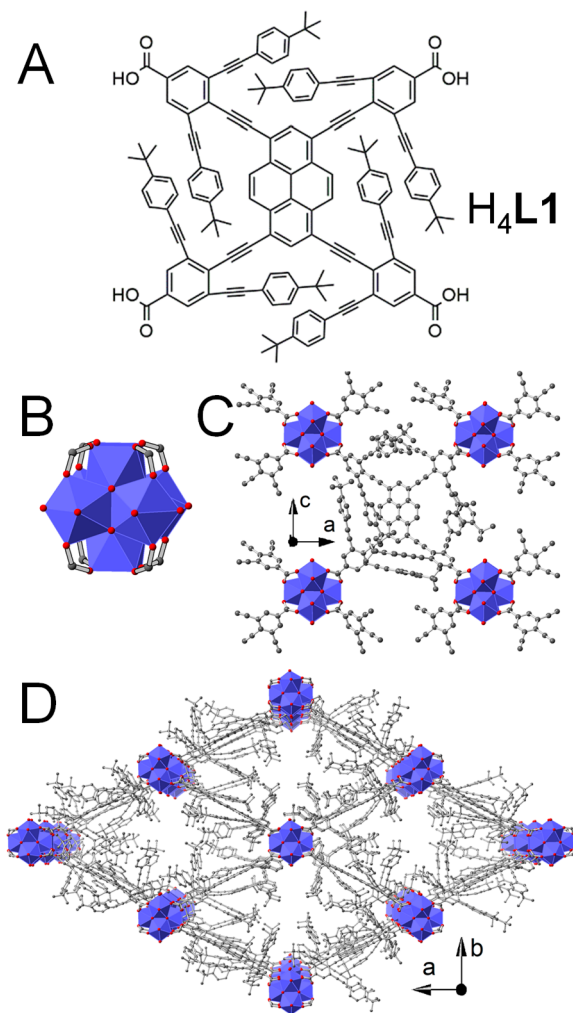


**Figure 1.** (A) Molecule  $\text{H}_4\text{L}1$  (featuring eight secondary alkyne groups). (B–D) Structure of  $\text{ZrL}1$ : the eight-connected  $\text{Zr}_6$  cluster (panel B) and views of the network along the  $b$  (panel C) and  $c$  axes (panel D). H atoms were omitted for clarity. Red spheres, O; gray, C; blue, Zr-based polyhedron.

Figure 2; details of the refinement are included in the SI). The PXRD of as-made  $\text{ZrL}1$  can be modeled after the NU-901-type

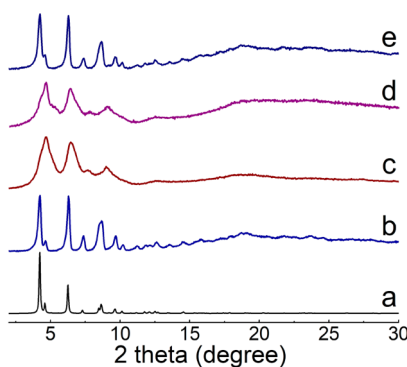


**Figure 2.** PXRD patterns ( $\text{Cu K}\alpha$ ,  $\lambda = 1.5418 \text{ \AA}$ ) for  $\text{ZrL}1$ : (a) calculated from the crystal structure model following PCN-606 topology; (b) measured from an as-made sample, covered by a DMF droplet during scanning; (c) from a fresh activated sample; (d) from an activated sample after being stored in air for 40 days; and (e) from (d) moistened by DMF.

structures reported by Farha, Stock, and Zhou,<sup>51–55</sup> which feature the **scu** topology based on tetratopic carboxyl linkers and eight-connected  $\text{Zr}_6\text{O}_8$  clusters (with four equatorial edges of the  $\text{Zr}_6$  octahedron sealed off by  $\text{H}_2\text{O}/\text{OH}^-$  species; Figure 1B). The identically oriented  $\text{Zr}_6\text{O}_8$  octahedra are arranged in a centered rectangular lattice to generate rhombus-shaped channels (Figure 1). The side-arm alkyne units are likely disordered in the channel region, but their well-defined vicinal positions within the linker favor intramolecular pathways for reactions among the alkyne units (e.g., at  $600^\circ\text{C}$ ; see below).

The **scu** net of the orthorhombic  $\text{ZrL}1$ , with its rhombus channels, compares instructively with the hexagonal NU-1000 and cubic NU-1100, with both built on tetratopic carboxyl linkers and  $\text{Zr}_6\text{O}_8$  nodes (Figures S5 and S6). The NU-1000 structure also features a (4,8)-connected net but consists of trigonal and hexagonal channels (i.e., the **csq** net). Compared with the rhombus channel of NU-901, the trigonal channel of NU-1000 is only half its size while the hexagonal ones are 3 times as large in cross-section. The targeted formation of the **scu** and **csq** nets in Zr-based MOFs has been reported.<sup>54,56,57</sup> The adoption of the **scu** net by  $\text{ZrL}1$  is likely driven by the steric effect from the rigid and bulky side arms of  $\text{L}1$ . For example, the smaller trigonal channel of the NU-1000-type structure (the **csq** net) may not accommodate the side arm volumes of  $\text{L}1$ . On the other hand, the NU-1100 structure features a (4,12)-connected **ftw** net, with the  $\text{Zr}_6\text{O}_8$  clusters being 12-connected in the ideal form.<sup>2,58</sup> The NU-1100 structures can exhibit twinning and disorder regarding linker orientations<sup>59</sup> and are generally solved in highly symmetric, cubic space groups, contrasting the orthorhombic  $\text{ZrL}1$  (Figure S8).

Elemental analysis found C (66.88%), H (4.88%), and N (0.40%) for activated  $\text{ZrL}1$ , which fits the formula  $\text{Zr}_6\text{O}_4(\text{OH})_8(\text{H}_2\text{O})_4(\text{C}_7\text{H}_5\text{O}_2)_{3.0}(\text{L}1)_{1.25}$  [calculated C (66.63%), H (4.85%)]. The benzoate ( $\text{C}_7\text{H}_5\text{O}_2$ )/ $\text{L}1$  ratio was also verified by the  $^1\text{H}$  NMR of the activated sample extracted into acetone- $d_6$  (using  $\text{K}_3\text{PO}_4$ ,  $\text{DCl}/\text{D}_2\text{O}$ ; Figure S4). Benzoate ions bonded to the residual open sites of the  $\text{Zr}_6$  clusters were also observed in the NU-901 prototype.<sup>51</sup> The 1:1.25 cluster/linker ratio indicates that out of the eight connecting sites of the  $\text{Zr}_6$  cluster in the **scu** net of  $\text{ZrL}1$ , only five were taken by the  $\text{L}1$  linker (with the other three being sealed off by the benzoate or  $\text{H}_2\text{O}/\text{OH}^-$  species). The significant linker deficiency (i.e.,  $3/8 = 37.5\%$ ) of  $\text{ZrL}1$  can be attributed to the steric repulsion from the bulky side arms of  $\text{L}1$ .

The thermogravimetric analysis (TGA; Figure S14a) of a powder of  $\text{H}_4\text{L}1$  suggests that the departure of the *t*-butyl and carboxyl units (accounting for 30.8% of weight loss) lasts up to  $500^\circ\text{C}$ , with a weight fraction of 51.4% remaining at  $900^\circ\text{C}$ . Similarly, TGA of the activated  $\text{ZrL}1$  sample (Figure S14b) reveals a distinct step of weight loss (of ca. 33%) of up to  $517^\circ\text{C}$ , corresponding to the departure of the water, benzoate, *t*-butyl, and carboxyl components, with the residue at  $900^\circ\text{C}$  (40.7%) far exceeding the  $\text{ZrO}_2$  weight.

Both flexibility and resilience were observed for the  $\text{ZrL}1$  framework. The PXRD of the activated  $\text{ZrL}1$  (i.e., a guestless sample obtained by solvent exchange with acetone and then evacuation) exhibits broadened peaks shifted to higher angles (pattern c, Figure 2), indicating lattice contraction and the partial loss of long-range order. The contracted phase, however, maintains significant gas uptake, exhibiting a typical type-I isotherm with a Langmuir surface area of  $486 \text{ m}^2/\text{g}$  in

$\text{CO}_2$  sorption at 195 K (Figures 3 and S15). The gas sorption behaviors reveal the ultramicroporosity of activated ZrL1,

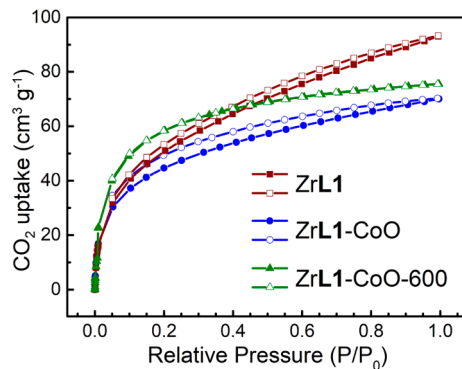


**Figure 3.**  $\text{CO}_2$  (195 K) adsorption and desorption isotherms for an activated ZrL1 sample (red graphs), ZrL1-CoO sample (blue graphs), and ZrL1-CoO-600 sample (green graphs).

which allows the selective penetration by  $\text{CO}_2$  (and not by  $\text{N}_2$ ) because of its smaller kinetic diameter, quadruple moment, and stronger thermal motion at 195 K (relative to 77 K for  $\text{N}_2$ ).<sup>60</sup>

Notably, activated ZrL1 is quite persistent (e.g., even after exposure to the moist air of Hong Kong for 40 days, its diffraction profile remains unchanged (Figure 2d)). The air stability may be partially ascribed to the bulky hydrophobic side arms that prevent water from eroding the metal node. Interestingly, upon contact with the DMF solvent, the contracted phase (i.e., activated ZrL1) reverts to the open phase of the as-made sample, as revealed by PXRD (pattern e, Figure 2; cf. pattern b). The swift recovery of the pristine phase is likely associated with the linker deficiency (i.e., 37.5%), leading to lower-connected  $\text{Zr}_6$  nodes (i.e., five-connected) and consequently more flexibility for framework dynamics.<sup>61</sup> Framework dynamics of Zr-MOF solids often arise from the supple topology,<sup>61,62</sup> linker flexibility,<sup>21,39,63,64</sup> and partial hydrolysis<sup>65</sup> of the carboxylate donors (e.g., switching from the bidentate bridging mode to the monodentate or uncoordinated mode). Further study is needed on how these factors contribute to the dynamic, breathing properties of ZrL1.

Unlike the strenuous (e.g., by vacuum deposition) grafting of metal carbonyl guests into other MOF matrixes,<sup>66–68</sup> the alkyne-functionalized ZrL1 solid (activated, orange-red) readily binds  $\text{Co}_2(\text{CO})_8$  from a THF solution to form the dark-brown ZrL1-Co<sub>2</sub>(CO)<sub>6</sub> solid. The characteristic, strong IR peaks at 2089, 2054, and 2028  $\text{cm}^{-1}$  (Figure 4b) of the CO stretches point to the known  $\mu_2$ -alkyne dicobalt hexacarbonyl complexes [ $\text{Co}_2(\text{CO})_6(\text{RC}\equiv\text{CR})$ ].<sup>69–71</sup> Compared with the yellow-fluorescing ZrL1 (emission peak at 585 nm for the activated, contracted phase and 572 nm for the open phase; Figure S10), ZrL1-Co<sub>2</sub>(CO)<sub>6</sub> is nonemissive.

The ZrL1-Co<sub>2</sub>(CO)<sub>6</sub> solid (brown) can be heated in air (e.g., at 75 °C for 3 h) to remove the CO ligands (IR evidence; Figure 4c). The resultant solid was denoted ZrL1-CoO because XPS reveals the Co 2p peak at 779.7 eV with distinct satellite features at ~786 eV indicative of the CoO species (Figure S11). Semiquantitative elemental analysis by EDX measurements (Figure S12) also indicate substantial cobalt content, with Zr/Co atomic ratios of 1:1.5 and 1:1.4 for ZrL1-Co<sub>2</sub>(CO)<sub>6</sub> and ZrL1-CoO, respectively. Further elemental analysis by ICP-OES quantifies the Zr/Co atomic ratio in

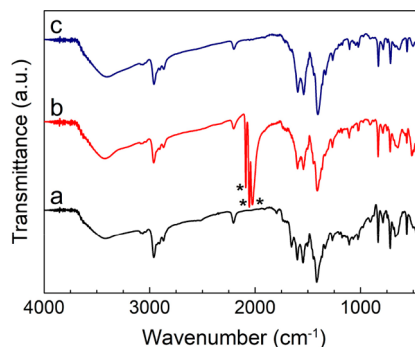


**Figure 4.** IR spectra for samples of (a) activated ZrL1, (b) ZrL1-Co<sub>2</sub>(CO)<sub>6</sub>, and (c) ZrL1-CoO.

ZrL1-CoO to be 1:1.49. With the above ZrL1 formula, a L1/Co ratio of 1:7.2 can be deduced, corresponding to about half (7.2/16 = 45%) of the eight alkyne side arms of each L1 linker being engaged as the [ $\text{Co}_2(\text{CO})_6(\text{RC}\equiv\text{CR})$ ] complex. The efficient uptake of  $\text{Co}_2(\text{CO})_8$  as enabled by the alkyne side arms is also highlighted by the poor  $\text{Co}_2(\text{CO})_8$  uptake (e.g., mostly limited to the external surfaces) of a MOF wherein the alkyne units were built into the linker backbone instead.<sup>72</sup> Comparison with other related MOFs (e.g., the isoreticular PCN-606<sup>53</sup> and NU-901<sup>73</sup>) with regard to metalation and catalysis, however, still warrants attention.

The ZrL1-CoO solid continues to feature a type-I isotherm in  $\text{CO}_2$  sorption (195 K, Figures 3 and S16), with a smaller Langmuir surface ( $340 \text{ m}^2 \text{ g}^{-1}$ ) than for activated ZrL1 ( $486 \text{ m}^2 \text{ g}^{-1}$ ), which is consistent with partial pore occupation by the CoO guests. ZrL1-CoO also exhibits greater hysteresis indicative of ultramicropore blocking by the CoO guests. PXRD of ZrL1-Co<sub>2</sub>(CO)<sub>6</sub> and ZrL1-CoO indicates that the host frameworks remain upstanding (Figure S13), although an unusually strong background (likely due to the CoO fluorescence<sup>74</sup>) largely obscures the diffraction signals. Notably, no diffraction peaks from CoO or other phases were observed, indicating the finely dispersed (and thus nondiffracting) nature of the CoO species within the MOF matrix; the fine distribution of CoO is also supported by SEM and TEM images (Figures S19–S22) of the ground samples of ZrL1-CoO, which reveal no large aggregated particles (e.g., of CoO) aside from the MOF matrix. The diffuse reflectance spectra (Figure S18) reveals the optical band gaps for the ZrL1, ZrL1-Co<sub>2</sub>(CO)<sub>6</sub>, and ZrL1-CoO solids to be about 2.19, 1.72, and 1.25 eV, respectively.

CoO is known to be a good electrocatalyst for the oxygen evolution reaction (OER) when strongly coupled with various carbon substrates including graphene and amorphous carbon.<sup>75–77</sup> To enhance charge transport for electrocatalysis applications, the ZrL1-CoO sample was heated to 600 °C for 3 h to carbonize the organic linkers (e.g., by cyclizing the alkyne units). The resulting black sample, ZrL1-CoO-600, remains porous (surface area,  $352 \text{ m}^2 \text{ g}^{-1}$ ; Figures 3 and S17), and the lack of distinct peaks in its PXRD pattern (Figure S23) indicates an amorphous structure with the Co species remaining highly dispersed (i.e., they do not aggregate into crystalline particles in the thermal treatment). In a 0.1 M KOH solution, the ZrL1-CoO-600 electrode gave a  $\eta_{10}$  of 544 mV and a small TS of 80 mV/dec (Figure S24), which are significantly enhanced over the control sample (i.e., without Co components) of ZrL1-600 ( $\eta > 577 \text{ mV}$  at  $1.0 \text{ mV/cm}^2$ , TS = 284 mV/dec). ZrL1-CoO-600 as an OER catalyst was thus

found to compare well with some of the cobalt-enabled MOF systems,<sup>78–80</sup> even though the linker structure, the metal loading, and thermal treatment conditions can be further tuned for better electrocatalytic properties.

## ■ ASSOCIATED CONTENT

### Supporting Information

The Supporting Information is available free of charge at <https://pubs.acs.org/doi/10.1021/acs.inorgchem.0c00328>.

General synthesis experimental details; <sup>1</sup>H NMR spectra, details of the structure simulation; MS, XPS, and FL spectra; LSV curves; and SEM/TEM images ([PDF](#))

## ■ AUTHOR INFORMATION

### Corresponding Authors

**Jun He** — School of Chemical Engineering and Light Industry, Guangdong University of Technology, Guangzhou 510006, Guangdong, P. R. China;  [orcid.org/0000-0001-7062-4001](https://orcid.org/0000-0001-7062-4001); Phone: 86 138 2211 8686; Email: [junhe@gdut.edu.cn](mailto:junhe@gdut.edu.cn)

**Zhengtao Xu** — Department of Chemistry, City University of Hong Kong, Kowloon, Hong Kong, P. R. China;  [orcid.org/0000-0002-7408-4951](https://orcid.org/0000-0002-7408-4951); Phone: 852 34424679; Email: [zhengtao@cityu.edu.hk](mailto:zhengtao@cityu.edu.hk)

### Authors

**Yingxue Diao** — Department of Materials Science and Engineering and Department of Chemistry, City University of Hong Kong, Kowloon, Hong Kong, P. R. China

**Jieying Hu** — Department of Materials Science and Engineering, City University of Hong Kong, Kowloon, Hong Kong, P. R. China; School of Chemical Engineering and Light Industry, Guangdong University of Technology, Guangzhou 510006, Guangdong, P. R. China

**Shengxian Cheng** — Department of Chemistry, City University of Hong Kong, Kowloon, Hong Kong, P. R. China

**Feixiang Ma** — Department of Mechanical Engineering, City University of Hong Kong, Kowloon, Hong Kong, P. R. China;  [orcid.org/0000-0002-2449-9139](https://orcid.org/0000-0002-2449-9139)

**Mu-Qing Li** — Department of Chemistry, City University of Hong Kong, Kowloon, Hong Kong, P. R. China

**Xiangzi Hu** — Department of Chemistry, City University of Hong Kong, Kowloon, Hong Kong, P. R. China

**Yang Yang Li** — Department of Materials Science and Engineering, City University of Hong Kong, Kowloon, Hong Kong, P. R. China;  [orcid.org/0000-0003-4153-9558](https://orcid.org/0000-0003-4153-9558)

Complete contact information is available at:

<https://pubs.acs.org/10.1021/acs.inorgchem.0c00328>

### Notes

The authors declare no competing financial interest.

## ■ ACKNOWLEDGMENTS

The work was supported by a GRF grant from the Research Grants Council of HKSAR (CityU 11306018) and an SRG grant from City University of Hong Kong (project 7004820).

## ■ REFERENCES

- (1) Zha, M.; Liu, J.; Wong, Y.-L.; Xu, Z. Extraction of palladium from nuclear waste-like acidic solutions by a metal-organic framework with sulfur and alkene functions. *J. Mater. Chem. A* **2015**, *3*, 3928–3934.

(2) Li, M.-Q.; Wong, Y.-L.; Lum, T.-S.; Sze-Yin Leung, K.; Lam, P. K. S.; Xu, Z. Dense thiol arrays for metal-organic frameworks: boiling water stability, Hg removal beyond 2 ppb and facile crosslinking. *J. Mater. Chem. A* **2018**, *6*, 14566–14570.

(3) Mon, M.; Lloret, F.; Ferrando-Soria, J.; Martí-Gastaldo, C.; Armentano, D.; Pardo, E. Selective and Efficient Removal of Mercury from Aqueous Media with the Highly Flexible Arms of a BioMOF. *Angew. Chem., Int. Ed.* **2016**, *55*, 11167–11172.

(4) He, Y.; Hou, Y.-L.; Wong, Y.-L.; Xiao, R.; Li, M.-Q.; Hao, Z.; Huang, J.; Wang, L.; Zeller, M.; He, J.; Xu, Z. Improving stability against desolvation and mercury removal performance of Zr(IV)-carboxylate frameworks by using bulky sulfur functions. *J. Mater. Chem. A* **2018**, *6*, 1648–1654.

(5) Yang, P.; Shu, Y.; Zhuang, Q.; Li, Y.; Gu, J. A robust MOF-based trap with high-density active alkyl thiol for the super-efficient capture of mercury. *Chem. Commun.* **2019**, *55*, 12972–12975.

(6) Kobielska, P. A.; Howarth, A. J.; Farha, O. K.; Nayak, S. Metal-organic frameworks for heavy metal removal from water. *Coord. Chem. Rev.* **2018**, *358*, 92–107.

(7) Gui, B.; Yee, K.-K.; Wong, Y.-L.; Yiu, S.-M.; Zeller, M.; Wang, C.; Xu, Z. Tackling poison and leach: catalysis by dangling thiopalladium functions within a porous metal-organic solid. *Chem. Commun.* **2015**, *51*, 6917–6920.

(8) Yee, K.-K.; Wong, Y.-L.; Zha, M.; Adhikari, R. Y.; Tuominen, M. T.; He, J.; Xu, Z. Room-temperature acetylene hydration by a Hg(II)-laced metal-organic framework. *Chem. Commun.* **2015**, *51*, 10941–10944.

(9) Wu, C.-D.; Hu, A.; Zhang, L.; Lin, W. A Homochiral Porous Metal-Organic Framework for Highly Enantioselective Heterogeneous Asymmetric Catalysis. *J. Am. Chem. Soc.* **2005**, *127*, 8940–8941.

(10) Wong, Y.-L.; Diao, Y.; He, J.; Zeller, M.; Xu, Z. A Thiol-Functionalized UiO-67-Type Porous Single Crystal: Filling in the Synthetic Gap. *Inorg. Chem.* **2019**, *58*, 1462–1468.

(11) Liu, D.-C.; Ouyang, T.; Xiao, R.; Liu, W.-J.; Zhong, D.-C.; Xu, Z.; Lu, T.-B. Anchoring CoII Ions into a Thiol-Laced Metal-Organic Framework for Efficient Visible-Light-Driven Conversion of CO<sub>2</sub> into CO. *ChemSusChem* **2019**, *12*, 2166–2170.

(12) Mon, M.; Rivero-Crespo, M. A.; Ferrando-Soria, J.; Vidal-Moya, A.; Boronat, M.; Leyva-Perez, A.; Corma, A.; Hernandez-Garrido, J. C.; Lopez-Haro, M.; Calvino, J. J.; Ragazzon, G.; Credi, A.; Armentano, D.; Pardo, E. Synthesis of Densely Packaged, Ultrasmall PtO<sub>2</sub> Clusters within a Thioether-Functionalized MOF: Catalytic Activity in Industrial Reactions at Low Temperature. *Angew. Chem., Int. Ed.* **2018**, *57*, 6186–6191.

(13) Mon, M.; Ferrando-Soria, J.; Grancha, T.; Fortea-Pérez, F. R.; Gascon, J.; Leyva-Pérez, A.; Armentano, D.; Pardo, E. Selective Gold Recovery and Catalysis in a Highly Flexible Methionine-Decorated Metal-Organic Framework. *J. Am. Chem. Soc.* **2016**, *138*, 7864–7867.

(14) Baek, J.; Rungtaweevoranit, B.; Pei, X.; Park, M.; Fakra, S. C.; Liu, Y.-S.; Matheu, R.; Alshimiri, S. A.; Alshehri, S.; Trickett, C. A.; Somorjai, G. A.; Yaghi, O. M. Bioinspired Metal-Organic Framework Catalysts for Selective Methane Oxidation to Methanol. *J. Am. Chem. Soc.* **2018**, *140*, 18208–18216.

(15) Sun, C.; Skorupskii, G.; Dou, J.-H.; Wright, A. M.; Dinca, M. Reversible Metalation and Catalysis with a Scorpionate-like Metalloc-ligand in a Metal-Organic Framework. *J. Am. Chem. Soc.* **2018**, *140*, 17394–17398.

(16) Feng, X.; Song, Y.; Li, Z.; Kaufmann, M.; Pi, Y.; Chen, J.; Xu, Z.; Zhong, L.; Wang, C.; Lin, W. Metal-Organic Framework Stabilizes a Low-Coordinate Iridium Complex for Catalytic Methane Borylation. *J. Am. Chem. Soc.* **2019**, *141*, 11196–11203.

(17) Han, B.; Wang, H.; Wang, C.; Wu, H.; Zhou, W.; Chen, B.; Jiang, J. Postsynthetic Metalation of a Robust Hydrogen-Bonded Organic Framework for Heterogeneous Catalysis. *J. Am. Chem. Soc.* **2019**, *141*, 8737–8740.

(18) He, J.; Zha, M.; Cui, J.; Zeller, M.; Hunter, A. D.; Yiu, S.-M.; Lee, S.-T.; Xu, Z. Convenient Detection of Pd(II) by a Metal-Organic

- Framework with Sulfur and Olefin Functions. *J. Am. Chem. Soc.* **2013**, *135*, 7807–7810.
- (19) Chen, B.; Wang, L.; Xiao, Y.; Fronczek, F. R.; Xue, M.; Cui, Y.; Qian, G. A luminescent metal-organic framework with Lewis basic pyridyl sites for the sensing of metal ions. *Angew. Chem., Int. Ed.* **2009**, *48*, 500–503.
- (20) Feng, J.-f.; Gao, S.-y.; Liu, T.-f.; Shi, J.; Cao, R. Preparation of dual-emitting Ln@UiO-66-hybrid films via electrophoretic deposition for ratiometric temperature sensing. *ACS Appl. Mater. Interfaces* **2018**, *10*, 6014–6023.
- (21) Hou, Y.-L.; Yee, K.-K.; Wong, Y.-L.; Zha, M.; He, J.; Zeller, M.; Hunter, A. D.; Yang, K.; Xu, Z. Metalation Triggers Single Crystalline Order in a Porous Solid. *J. Am. Chem. Soc.* **2016**, *138*, 14852–14855.
- (22) Zhou, X.-P.; Xu, Z.; Zeller, M.; Hunter, A. D. Reversible uptake of HgCl<sub>2</sub> in a porous coordination polymer based on the dual functions of carboxylate and thioether. *Chem. Commun.* **2009**, 5439–5441.
- (23) Bloch, W. M.; Burgun, A.; Coghlan, C. J.; Lee, R.; Coote, M. L.; Doonan, C. J.; Sumby, C. J. Capturing snapshots of post-synthetic metallation chemistry in metal-organic frameworks. *Nat. Chem.* **2014**, *6*, 906–912.
- (24) He, Y.; Huang, M.; Deng, X.; Cheng, S.; Wong, Y.-L.; Hou, Y.-L.; He, J.; Zeller, M.; Xu, Z. Janus triple tripods build up a microporous manifold for HgCl<sub>2</sub> and I<sub>2</sub> uptake. *Chem. Commun.* **2019**, *55*, 5091–5094.
- (25) Sikma, R. E.; Kunal, P.; Dunning, S. G.; Reynolds, J. E.; Lee, J. S.; Chang, J.-S.; Humphrey, S. M. Organoarsine Metal-Organic Framework with cis-Diarsine Pockets for the Installation of Uniquely Confined Metal Complexes. *J. Am. Chem. Soc.* **2018**, *140*, 9806–9809.
- (26) Dunning, S. G.; Nandra, G.; Conn, A. D.; Chai, W.; Sikma, R. E.; Lee, J. S.; Kunal, P.; Reynolds, J. E., III; Chang, J.-S.; Steiner, A.; Henkelman, G.; Humphrey, S. M. A Metal-Organic Framework with Cooperative Phosphines That Permit Post-Synthetic Installation of Open Metal Sites. *Angew. Chem., Int. Ed.* **2018**, *57*, 9295–9299.
- (27) Zhou, X.-P.; Xu, Z.; Zeller, M.; Hunter, A. D.; Chui, S. S.-Y.; Che, C.-M. Coordination Networks from a Bifunctional Molecule Containing Carboxyl and Thioether Groups. *Inorg. Chem.* **2008**, *47*, 7459–7461.
- (28) He, J.; Yang, C.; Xu, Z.; Zeller, M.; Hunter, A. D.; Lin, J. Building thiol and metal-thiolate functions into coordination nets: Clues from a simple molecule. *J. Solid State Chem.* **2009**, *182*, 1821–1826.
- (29) He, J.; Cheng, S.; Xu, Z. Sulfur Chemistry for Stable and Electroactive Metal-Organic Frameworks: The Crosslinking Story. *Chem. - Eur. J.* **2019**, *25*, 1–10.
- (30) Resa, S.; Miguel, D.; Guisan-Ceinos, S.; Mazzeo, G.; Choquillo-Lazarte, D.; Abbate, S.; Crovetto, L.; Cardenas, D. J.; Carreno, M. C.; Ribagorda, M.; Longhi, G.; Mota, A. J.; Alvarez de Cienfuegos, L.; Cuerva, J. M. Sulfoxide-Induced Homochiral Folding of ortho-Phenylene Ethynylanes (o-OPEs) by Silver(I) Templating: Structure and Chiroptical Properties. *Chem. - Eur. J.* **2018**, *24*, 2653–2662.
- (31) Martin-Lasanta, A.; Alvarez de Cienfuegos, L.; Johnson, A.; Miguel, D.; Mota, A. J.; Orte, A.; Ruedas-Rama, M. J.; Ribagorda, M.; Cardenas, D. J.; Carmen Carreno, M.; Echavarren, A. M.; Cuerva, J. M. Novel ortho-OPE metallocoldamers: binding-induced folding promoted by nucleating Ag(I)-alkyne interactions. *Chem. Sci.* **2014**, *5*, 4582–4591.
- (32) Das, A.; Dash, C.; Celik, M. A.; Yousufuddin, M.; Frenking, G.; Dias, H. V. R. Tris(alkyne) and Bis(alkyne) Complexes of Coinage Metals: Synthesis and Characterization of (cyclooctyne)3M<sup>+</sup> (M = Cu, Ag) and (cyclooctyne)2Au<sup>+</sup> and Coinage Metal (M = Cu, Ag, Au) Family Group Trends. *Organometallics* **2013**, *32*, 3135–3144.
- (33) Fluegge, S.; Anoop, A.; Goddard, R.; Thiel, W.; Fuerstner, A. Structure and Bonding in Neutral and Cationic 14-Electron Gold Alkyne π Complexes. *Chem. - Eur. J.* **2009**, *15*, 8558–8565.
- (34) Kunze, A.; Balalaie, S.; Gleiter, R.; Rominger, F. π-Prisms – flexible hosts for metal ions. *Eur. J. Org. Chem.* **2006**, *2006*, 2942–2955.
- (35) Sappa, E. Complexes of transition metal carbonyls with alkynes. Closo- and nido-pentagonal bipyramidal clusters. *J. Organomet. Chem.* **1999**, *573*, 139–155.
- (36) Gervasio, G.; Sappa, E.; Secco, A. Advances in the chemistry of alkyne-substituted homo- and heterometallic carbonyl clusters of the iron, cobalt and nickel triads. An update. *J. Organomet. Chem.* **2014**, *751*, 111–152.
- (37) Cui, J.; Wong, Y.-L.; Zeller, M.; Hunter, A. D.; Xu, Z. Pd Uptake and H<sub>2</sub>S Sensing by an Amphoteric Metal-Organic Framework with a Soft Core and Rigid Side Arms. *Angew. Chem., Int. Ed.* **2014**, *53*, 14438–14442.
- (38) Hu, J.-Y.; Sun, Y.-Q.; Xiao, R.; Cheng, S.; He, J.; Zeller, M.; Wong, W.-Y.; Xu, Z. Symmetrically backfolded molecules emulating the self-similar features of a Sierpinski triangle. *Org. Biomol. Chem.* **2019**, *17*, 6032–6037.
- (39) Hou, Y.-L.; Li, M.-Q.; Cheng, S.; Diao, Y.; Vilela, F.; He, Y.; He, J.; Xu, Z. Dramatic improvement of stability by in situ linker cyclization of a metal-organic framework. *Chem. Commun.* **2018**, *54*, 9470–9473.
- (40) Yang, C.; Wong, Y.-L.; Xiao, R.; Zeller, M.; Hunter, A. D.; Yiu, S.-M.; Xu, Z. Complex Metal-Organic Frameworks from Symmetrically Backfolded Dendrimers. *ChemistrySelect* **2016**, *1*, 4075–4081.
- (41) Sun, Y.-Q.; Yang, C.; Xu, Z.; Zeller, M.; Hunter, A. D. Networks of Hexagonal Hierarchy from a Self-Similar Tritopic Molecule. *Cryst. Growth Des.* **2009**, *9*, 1663–1665.
- (42) Xu, Z.; Sun, Y.-Q.; He, J.; Zeller, M.; Hunter, A. D. *The Concept and Use of a Class of Branchy Molecules with Centripetal Self-Similarity*; Nova Science Publishers, Inc.: Hauppauge, NY, 2008.
- (43) Sun, Y.-Q.; He, J.; Xu, Z.; Huang, G.; Zhou, X.-P.; Zeller, M.; Hunter, A. D. Centripetal molecules as multifunctional building blocks for coordination networks. *Chem. Commun.* **2007**, 4779–4781.
- (44) Woods, C. R.; Benaglia, M.; Toyota, S.; Hardcastle, K.; Siegel, J. S. Trinuclear copper(I)-bipyridine triskelion: template/bascule control of coordination complex stereochemistry in a trefoil knot precursor. *Angew. Chem., Int. Ed.* **2001**, *40*, 749–751.
- (45) Nandy, R.; Subramoni, M.; Varghese, B.; Sankararaman, S. Intramolecular p-Stacking Interaction in a Rigid Molecular Hinge Substituted with 1-(Pyrenylethynyl) Units. *J. Org. Chem.* **2007**, *72*, 938–944.
- (46) Narayanan, V.; Sankararaman, S.; Hopf, H. Synthesis of shape-persistent polyal dendrimers - facile entry to polyene and polyyne dendrimers. *Eur. J. Org. Chem.* **2005**, *2005*, 2740–2746.
- (47) Marsden, J. A.; O'Connor, M. J.; Haley, M. M. Synthesis and Characterization of Multiply Fused Dehydrobenzoannulenoannulene Topologies. *Org. Lett.* **2004**, *6*, 2385–2388.
- (48) Bradshaw, J. D.; Guo, L.; Tessier, C. A.; Youngs, W. J. Planar Platinum Metallacyclines Containing One and Two Trialkyne Pockets. *Organometallics* **1996**, *15*, 2582–2584.
- (49) Laskoski, M.; Steffen, W.; Morton, J. G. M.; Smith, M. D.; Bunz, U. H. F. Synthesis and structural characterization of organometallic cyclones: novel nanoscale, carbon-rich topologies. *J. Organomet. Chem.* **2003**, *673*, 25–39.
- (50) Yang, W.; Longhi, G.; Abbate, S.; Lucotti, A.; Tommasini, M.; Villani, C.; Catalano, V. J.; Lykhin, A. O.; Varganov, S. A.; Chalifoux, W. A. Chiral Peropyrene: Synthesis, Structure, and Properties. *J. Am. Chem. Soc.* **2017**, *139*, 13102–13109.
- (51) Kung, C.-W.; Wang, T. C.; Mondloch, J. E.; Fairen-Jimenez, D.; Gardner, D. M.; Bury, W.; Klinsporn, J. M.; Barnes, J. C.; Van Duyne, R.; Stoddart, J. F.; Wasielewski, M. R.; Farha, O. K.; Hupp, J. T. Metal–Organic Framework Thin Films Composed of Free-Standing Acicular Nanorods Exhibiting Reversible Electrochromism. *Chem. Mater.* **2013**, *25*, 5012–5017.
- (52) Lammert, M.; Reinsch, H.; Murray, C. A.; Wharmby, M. T.; Terraschke, H.; Stock, N. Synthesis and structure of Zr(IV)- and Ce(IV)-based CAU-24 with 1,2,4,5-tetrakis(4-carboxyphenyl)-benzene. *Dalton Trans.* **2016**, *45*, 18822–18826.
- (53) Pang, J.; Yuan, S.; Du, D.; Lollar, C.; Zhang, L.; Wu, M.; Yuan, D.; Zhou, H.-C.; Hong, M. Flexible Zirconium MOFs as Bromine-

- Nanocontainers for Bromination Reactions under Ambient Conditions. *Angew. Chem., Int. Ed.* **2017**, *56*, 14622–14626.
- (54) Islamoglu, T.; Otake, K.-i.; Li, P.; Buru, C. T.; Peters, A. W.; Akpinar, I.; Garibay, S. J.; Farha, O. K. Revisiting the structural homogeneity of NU-1000, a Zr-based metal-organic framework. *CrystEngComm* **2018**, *20*, 5913–5918.
- (55) Lyu, J.; Zhang, X.; Otake, K.-i.; Wang, X.; Li, P.; Li, Z.; Chen, Z.; Zhang, Y.; Wasson, M. C.; Yang, Y.; Bai, P.; Guo, X.; Islamoglu, T.; Farha, O. K. Topology and porosity control of metal-organic frameworks through linker functionalization. *Chem. Sci.* **2019**, *10*, 1186–1192.
- (56) Webber, T. E.; Liu, W.-G.; Desai, S. P.; Lu, C. C.; Truhlar, D. G.; Penn, R. L. Role of a Modulator in the Synthesis of Phase-Pure NU-1000. *ACS Appl. Mater. Interfaces* **2017**, *9*, 39342–39346.
- (57) Pang, J.; Yuan, S.; Qin, J.; Liu, C.; Lollar, C.; Wu, M.; Yuan, D.; Zhou, H. C.; Hong, M. Control the Structure of Zr-Tetracarboxylate Frameworks through Steric Tuning. *J. Am. Chem. Soc.* **2017**, *139*, 16939–16945.
- (58) Gutov, O. V.; Bury, W.; Gomez-Gualdrón, D. A.; Krungleviciute, V.; Fairen-Jimenez, D.; Mondloch, J. E.; Sarjeant, A. A.; Al-Juaid, S. S.; Snurr, R. Q.; Hupp, J. T.; Yildirim, T.; Farha, O. K. Water-Stable Zirconium-Based Metal-Organic Framework Material with High-Surface Area and Gas-Storage Capacities. *Chem. - Eur. J.* **2014**, *20*, 12389–12393.
- (59) Oien-Odegaard, S.; Shearer, G. C.; Wragg, D. S.; Lillerud, K. P. Pitfalls in metal-organic framework crystallography: towards more accurate crystal structures. *Chem. Soc. Rev.* **2017**, *46*, 4867–4876.
- (60) Kim, K. C.; Yoon, T.-U.; Bae, Y.-S. Applicability of using CO<sub>2</sub> adsorption isotherms to determine BET surface areas of microporous materials. *Microporous Mesoporous Mater.* **2016**, *224*, 294–301.
- (61) Zhang, Y.; Zhang, X.; Lyu, J.; Otake, K.-i.; Wang, X.; Redfern, L. R.; Malliakas, C. D.; Li, Z.; Islamoglu, T.; Wang, B.; Farha, O. K. A Flexible Metal-Organic Framework with 4-Connected Zr<sub>6</sub> Nodes. *J. Am. Chem. Soc.* **2018**, *140*, 11179–11183.
- (62) Qin, J. S.; Yuan, S.; Alsalme, A.; Zhou, H. C. Flexible Zirconium MOF as the Crystalline Sponge for Coordinative Alignment of Dicarboxylates. *ACS Appl. Mater. Interfaces* **2017**, *9*, 33408–33412.
- (63) Deria, P.; Gomez-Gualdrón, D. A.; Bury, W.; Schaeff, H. T.; Wang, T. C.; Thallapally, P. K.; Sarjeant, A. A.; Snurr, R. Q.; Hupp, J. T.; Farha, O. K. Ultraporous, Water Stable, and Breathing Zirconium-Based Metal-Organic Frameworks with ftw Topology. *J. Am. Chem. Soc.* **2015**, *137*, 13183–13190.
- (64) Wang, S.; Xhaferaj, N.; Wahiduzzaman, M.; Oyekan, K.; Li, X.; Wei, K.; Zheng, B.; Tissot, A.; Marrot, J.; Shepard, W.; Martineau-Corcos, C.; Filinchuk, Y.; Tan, K.; Maurin, G.; Serre, C. Engineering Structural Dynamics of Zirconium Metal-Organic Frameworks Based on Natural C<sub>4</sub> Linkers. *J. Am. Chem. Soc.* **2019**, *141*, 17207–17216.
- (65) Krause, S.; Bon, V.; Stoeck, U.; Senkovska, I.; Tobbens, D. M.; Wallacher, D.; Kaskel, S. A Stimuli-Responsive Zirconium Metal-Organic Framework Based on Supramolecular Design. *Angew. Chem., Int. Ed.* **2017**, *56*, 10676–10680.
- (66) Saito, M.; Toyao, T.; Ueda, K.; Kamegawa, T.; Horiuchi, Y.; Matsuoka, M. Effect of pore sizes on catalytic activities of arenetricarbonyl metal complexes constructed within Zr-based MOFs. *Dalton Trans* **2013**, *42*, 9444–9447.
- (67) Larabi, C.; Nielsen, P. K.; Helveg, S.; Thieuleux, C.; Johansson, F. B.; Brorson, M.; Quadrelli, E. A. Bulk Hydrodesulfurization Catalyst Obtained by Mo(CO)<sub>6</sub> Grafting on the Metal-Organic Framework Ni<sub>2</sub>(2,5-dihydroxoterephthalate). *ACS Catal.* **2012**, *2*, 695–700.
- (68) Chavan, S.; Vitillo, J. G.; Larabi, C.; Quadrelli, E. A.; Dietzel, P. D. C.; Bordiga, S. Functionalization of CPO-27-Ni through metal hexacarbonyls: The role of open Ni<sup>2+</sup> sites. *Microporous Mesoporous Mater.* **2012**, *157*, 56–61.
- (69) Ruan, Z.; Rong, W.; Li, Q.; Li, Z. Oxygen as the growth enhancer of carbon nanotubes in solid-state pyrolysis of organometallic precursors. *Carbon* **2015**, *87*, 338–346.
- (70) Boyle, N. M.; Coleman, A. C.; Long, C.; Ronayne, K. L.; Browne, W. R.; Feringa, B. L.; Pryce, M. T. Evidence for cobalt-cobalt bond homolysis and wavelength-dependent CO loss in ( $\mu$ 2-alkyne)-Co<sub>2</sub>(CO)<sub>6</sub> complexes. *Inorg. Chem.* **2010**, *49*, 10214–10216.
- (71) Ji, Y.; Riera, A.; Verdaguer, X. Asymmetric Intermolecular Pauson-Khand Reaction of Symmetrically Substituted Alkynes. *Org. Lett.* **2009**, *11*, 4346–4349.
- (72) Burrows, A. D.; Fisher, L. C.; Hodgson, D.; Mahon, M. F.; Cessford, N. F.; Düren, T.; Richardson, C.; Rigby, S. P. The synthesis, structures and reactions of zinc and cobalt metal-organic frameworks incorporating an alkyne-based dicarboxylate linker. *CrystEngComm* **2012**, *14*, 188–192.
- (73) Garibay, S. J.; Iordanov, I.; Islamoglu, T.; DeCoste, J. B.; Farha, O. K. Synthesis and functionalization of phase-pure NU-901 for enhanced CO<sub>2</sub>adsorption: the influence of a zirconium salt and modulator on the topology and phase purity. *CrystEngComm* **2018**, *20*, 7066–7070.
- (74) Fransen, M. J. On the influence of generator and detector settings in X-ray powder diffractometry. *Adv. X-ray Anal.* **2005**, *48*, 143–149.
- (75) Mao, S.; Wen, Z.; Huang, T.; Hou, Y.; Chen, J. High-performance bi-functional electrocatalysts of 3D crumpled graphene–cobalt oxide nanohybrids for oxygen reduction and evolution reactions. *Energy Environ. Sci.* **2014**, *7*, 609–616.
- (76) Ullah, N.; Zhao, W.; Lu, X.; Oluigbo, C. J.; Shah, S. A.; Zhang, M.; Xie, J.; Xu, Y. In situ growth of M-MO (M = Ni, Co) in 3D graphene as a competent bifunctional electrocatalyst for OER and HER. *Electrochim. Acta* **2019**, *298*, 163–171.
- (77) Xu, D.; Mu, C.; Xiang, J.; Wen, F.; Su, C.; Hao, C.; Hu, W.; Tang, Y.; Liu, Z. Carbon-Encapsulated Co<sub>3</sub>O<sub>4</sub>@CoO@Co Nanocomposites for Multifunctional Applications in Enhanced Long-life Lithium Storage, Supercapacitor and Oxygen Evolution Reaction. *Electrochim. Acta* **2016**, *220*, 322–330.
- (78) Tripathy, R. K.; Samantara, A. K.; Behera, J. N. A cobalt metal-organic framework (Co-MOF): a bi-functional electro active material for the oxygen evolution and reduction reaction. *Dalton Trans* **2019**, *48*, 10557–10564.
- (79) Ma, T. Y.; Dai, S.; Jaroniec, M.; Qiao, S. Z. Metal-organic framework derived hybrid Co<sub>3</sub>O<sub>4</sub>-carbon porous nanowire arrays as reversible oxygen evolution electrodes. *J. Am. Chem. Soc.* **2014**, *136*, 13925–13931.
- (80) Wang, S.; Hou, Y.; Lin, S.; Wang, X. Water oxidation electrocatalysis by a zeolitic imidazolate framework. *Nanoscale* **2014**, *6*, 9930–9934.